Design Procedure of a Turbopump Test Bench

Julian D Pauw, Lucrezia Veggi, Bernd Wagner, Joydip Mondal, Maximilian Klotz, Oskar Haidn

Design Procedure of a Turbopump Test Bench

Julian D. Pauw[1]*, Lucrezia Veggi[1], Bernd Wagner[2], Joydip Mondal[1,3], Maximilian Klotz[1], Oskar J. Haidn[1]

ISROMAC 2017

International Symposium on Transport Phenomena and Dynamics of Rotating Machinery

Maui, Hawaii

December 16-21, 2017

Abstract

The high complexity of turbopumps for liquid rocket engines and their demanding requirements necessitate that their design process is accompanied by extensive experimental investigations and validation tests. This paper presents the design procedure for a rocket turbopump test bench, where water is used as a surrogate for the cryogenic fluids usually used in rocket engines. Scaling methods, that allow for a comparison of tests under varying conditions, are reviewed from literature and applied to derive the necessary dimensions of the test bench. The resulting test bench design is shown in detail and its capabilities to support the turbopump design process are assessed. Further, the operational envelope of the derived test bench design is evaluated with respect to later tests of different pumps.

Keywords

turbopump — liquid oxygen scaling — test bench design

[1] *Technical University of Munich, Department of Mechnical Engineering, Chair of Turbomachinery and Flight Propulsion, Divison Space Propulsion, Munich, Germany*

[2] *Institute of Space Propulsion Lampoldshausen, German Aerospace Center (DLR), Hardthausen, Germany*

[3] *Cryogenic Engineering Centre, Indian Institute of Technology Kharagpur, India*

*__Corresponding author__: julian.pauw@ltf.mw.tum.de

1. INTRODUCTION

The turbopumps of a liquid rocket engine (LRE) supply the combustion devices with fuel and oxidizer at high mass flow rates and at a high pressure level. Typically, fuel and oxidizer are pumped by separate pumps. The turbopumps increase the pressure from a low pressure level in the tank to a high pressure level needed for the combustion process. Consequently, the turbopumps are a substantial part of the rocket engine. The dimension and the performance of the turbopumps depend highly on the desired engine operation point, the engine cycle and the requirements of the combustion chamber.

The work performed at the Division Space Propulsion of the Technical University of Munich (TUM) is embedded into the research project KonRAT, i.e. rocket propulsion engine components for applications in aerospace transportation systems. The project aims at establishing competences in the development of turbopumps. [1, 2, 3, 4, 5]. Key objective at the Division Space Propulsion, TUM, is the investigation of the design process of turbopumps and the investigation of fluid phenomena. Both parts are carried out numerically as well as experimentally.

The Division Space Propulsion, TUM, has established a design process for rocket engine turbo pumps based on well-known literature and commercially available software tools [1]. In order to fully understand all design parameters and to ensure that those parameters desired can be reached, experimental validation of those design parameters is an indispensable step in the design loop of every rocket engine turbopump.

The fuel and the oxidizer of cryogenic liquid rocket engines are stored in liquid state under boiling conditions on-board the launcher and thus ground tests with cryogenic fluids are of very complex nature. Besides the difficult generation and storage of the cryogenic fluids, the demands on the turbopump under development are very high as the design needs to withstand high temperature loads and it needs to take into consideration material choices for cryogenic temperatures for every tests. Consequently, tests with fluids that are liquid at ambient temperature are highly desirable. Further, it would be beneficial to perform tests at lower rotational speeds without loosing information on the flow behaviour inside the pump. Test benches operated with water at ambient temperature have been established as a very good solution to this problem. A drawback of tests at ambient temperature with water is that the cavitational behaviour of turbopumps cannot be captured. Especially, the so called thermodynamic suppression head (TSH), an effect that can be observed at tests with cryogenic fluids, is not present at ambient temperature tests with water. A solution is provided by the findings of several research groups which show that similarity of the cavitational performance can be reached by heating the water up [6, 7, 8, 9, 10, 11].

In literature, many different scaling and similarity methods are present. This paper will present a set of those methods based on a literature survey and makes use of the methods in order to define the operating conditions of a test bench for a liquid oxygen turbo pump developed at TUM. The derived test bench will be shown in detail and its properties will be evaluated for later usage. This is mostly done by making use of a numerical test bench representation in the commercially

available software tool *EcosimPro*®. In order to be able to use the test bench for other configurations as well, an outlook on the generalized operational envelope of the test bench will complete this paper, so that the possible use for future test campaigns with different configurations can be estimated.

2. SCALING METHODS

In order to test a pump in a test facility at conditions that differ from the normal operating conditions, the similarity of the flow passing through the pumps needs to be established both at the test bench and at the operational conditions. According to [12, 13, 14], this similarity can be reached if four different parameters are comparable: (1) the geometry under investigation, (2) a comparable establishment of velocity triangles at pump inlet and outlet, (3) a similar dynamic behaviour of the pump and (4) comparable thermodynamic properties of the fluids.

Following Sigloch [13, 14], geometric comparability of two turbo machines is fulfilled if the dimensions of the parts conducting the flow follow a certain ratio in all spatial dimensions. This offers not only comparable interaction of the fluid with the static and dynamic parts of the machine, but also yields similar velocity triangles at every corresponding point for friction-free conditions because the velocity vectors are then governed by passage dimensions and the rotational speed only. It is important to make sure that not only the rotor and blade geometries are comparable, but also the gap geometries and clearance distances between rotor and housing.

$$\lambda_{geometry} = \frac{\text{dimension of prototype}}{\text{dimension of model}} = \frac{X_m}{X_a} \tag{1}$$

$$\lambda_{velocity} = \frac{\text{velocities of prototype}}{\text{velocities of model}} = \frac{v_m}{v_a} \tag{2}$$

In the case of single-phase flows, i.e. in the case of non-cavitating flows, the forces acting on the pump are the following: inertia forces, pressure forces, viscous forces and the gravitational force. Additionally, forces resulting from the elasticity of the mechanical system, especially the shaft, can act on the pump components. The flow through two different pumps can only be considered similar if the ratio of the forces acting on these pumps is constant in all spatial directions.

$$\lambda_{Force} = \frac{\text{forces at prototype}}{\text{forces at model}} = \frac{F_m}{F_a} \tag{3}$$

The forces acting in pumps with single-phase flows can be related by the Froude number, the Reynolds number and the Euler number. These characteristic numbers should be the same for the model and the prototype.
The Froude number is defined as the ratio of inertia forces to gravitational forces. It is commonly used in hydro-mechanics to model flows with free surfaces where gravitational forces have a large impact.

$$\mathrm{Fr} = \frac{\text{inertia force}}{\text{gravitational force}} = \frac{\mathrm{v}^2}{\mathrm{gL_c}} \tag{4}$$

The Reynolds number relates between the acting inertia forces and the viscous forces. Equivalent Reynolds numbers predict a similar development of boundary layers inside two compared pumps. The generation of boundary layers is closely linked to the surface roughness of the parts that conduct the flow. Especially for geometrically scaled models it is difficult to generate a comparable surface roughness of all pump components. For the purpose of comparing different radial machines, the Reynolds number is often defined as the product of peripheral velocity U_3 at the impeller outlet and the corresponding tip radius R_3 divided by the kinematic viscosity υ. When comparing the scaled measurements in detail, it is strongly recommended to calculate the Reynolds number locally to guarantee comparable boundary layers all over the pump [14, 13, 15, 16].

$$\mathrm{Re} = \frac{\text{inertia force}}{\text{viscous force}} = \frac{\mathrm{U_3 R_{t,3}}}{\upsilon} = \frac{\omega \mathrm{R_{t,3}^2}}{\upsilon} \tag{5}$$

The Euler number describes the ratio between pressure forces and inertia forces. For the scaling of pumps, it is inevitable to keep the Euler number the same for model and prototype.

$$\mathrm{Eu} = \frac{\text{pressure force}}{\text{inertia force}} = \frac{\Delta \mathrm{p}}{\rho \mathrm{v}^2} \tag{6}$$

Further, the thermal properties of the fluids, i.e. the specific heat, the enthalpy and the thermal diffusivity, largely influence the flow characteristics. This is especially true for machines that exhibit a large pressure difference. It is advisable to make use of fluids with comparable properties and to closely track property changes.

The above scaling methods need to be incorporated in order to design a test bench that can be used to test a LOX turbopump with water. For ground tests of liquid rocket engine turbopumps, the gravitational effects are negligible. The differences in height and the resulting effects are comparably small. The Froude scaling is thus irrelevant. The Reynolds scaling is of high importance. At least for this application, it is sufficient to achieve fully turbulent conditions in the model and the prototype because the boundary layers that develop at turbulent conditions are assumed to be comparable. Fully turbulent conditions can be considered for $Re_{t,3} > 10^6$. Due to the high rotational speeds of liquid rocket engine turbopumps, this requirement can be fulfilled without any problems. Figure 1 sums up the properties that need to be scaled for liquid rocket engine turbopumps.
Obeying the above given similarity conditions, the operating properties can be transferred between model and prototype

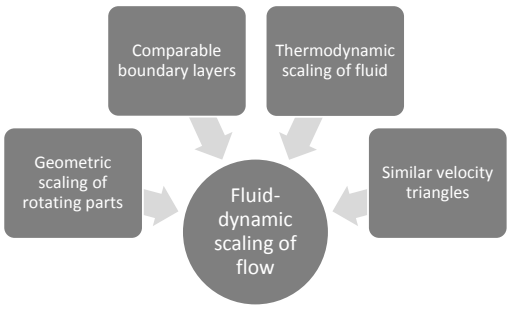

Figure 1. Comparable properties for fluid-dynamic similarity

with the help of well-known scaling laws for pumps[14].

For the volume flow rate:

$$\frac{Q_m}{N_m {D_{t,m}}^3} = \frac{Q_a}{N_a {D_{t,a}}^3} \tag{7}$$

For the head rise:

$$\frac{H_m}{{N_m}^2 {D_{t,m}}^2} = \frac{H_a}{{N_a}^2 {D_{t,a}}^2} \tag{8}$$

For the input power:

$$\frac{P_m}{{N_m}^3 {D_{t,m}}^5 \rho_m} = \frac{P_a}{{N_a}^3 {D_{t,a}}^5 \rho_a} \tag{9}$$

2.1 Scaling of Cavitation Phenomena

The scaling methodology above is valid for ideal fluids, i.e. non-cavitating single-phase flows. In operational regimes where cavitation at the pump blades occurs, a two-phase flow is present as a phase change is triggered by a pressure drop where the local fluid pressure is below the vapour pressure of the fluid. Usually, a certain amount of cavitation can be accepted for every pump, but excessive cavitation results in a head break down of the whole pump and defines an operational limit of the pump when the local static pressure is much smaller than the vapor pressure of the pumped liquid. In rocket engine turbopumps, cavitation usually first occurs at the leading-edge of the inducer and it is for most applications best described by heterogeneous nucleation due to fluid impurities [17]. By definition, the net positive suction head (NPSH) calculates to the difference between the total pressure and the fluid's vapor pressure at the inlet divided by the local density of the fluid. [18].

$$\text{NPSH} = \frac{P_{st} - P_v}{\rho g} \tag{10}$$

The required net positive suction head (NPSH_R) is commonly defined as the point where operation of the pump is still feasible. The minimal required NPSH_R has to be smaller than the available NPSH_A.

$$\text{NPSH}_R \leq \text{NPSH}_A \tag{11}$$

In order to show comparable behaviour with water as a surrogate compared to cryogenic fluids in terms of cavitation, it is necessary to match the same flow coefficient φ as well as the cavitation number σ [14, 15].

$$\varphi = \frac{2Q}{AD_t\omega} \tag{12}$$

$$\sigma = \frac{(p_{st} - p_v)}{2\rho_l D_t^2 \omega^2} \tag{13}$$

However, in experiments with several fluids, especially with cryogenic fluids, that operate close to their critical point like liquid hydrogen and liquid oxygen, it was possible to observe that the inducers of pumps are operating without cavitation at NPSH values smaller than the NPSH_R which would be expected for an ideal fluid. This effect is commonly called thermal suppression head (TSH). By definition, the TSH calculates to the difference between the available NPSH_A and the $\text{NPSH}_{ideal\,fluid}$ that would be expected for an ideal fluid. $\text{NPSH}_{ideal\,fluid}$ equals the NPSH_{tank} minus friction losses in the inlet tubing [18].

$$\text{TSH} = \text{NPSH}_{available} - \text{NPSH}_{ideal\,fluid} \tag{14}$$

The mechanism of bubble formation, growth and collapse in cavitation depends largely on the instantaneous heat transfer between the bubble and the surrounding fluid, the size of the pump and the speed of the pump. Thus, additional scaling methods are needed to allow for a prediction of the mechanisms related to thermodynamic effects. Several parameters and models have been suggested in order to describe and predict the occurrence of cavitation in this regard [19, 12, 20, 21, 22, 23].

Brennen [24], by simply looking at a heat balance between the vapor and liquid phases, established a dimensional parameter that, as he claimed, should be identical for replicating identical cavitation behavior in two liquids. He assumed that the heat-transfer between the bubble and its surrounding is of conductive nature. The developed parameter Σ is widely used. Thereby, he tried to show the different ranges within which the cavitation behavior of different fluids resembled the cavitation behaviour of water.

$$\Sigma = \frac{\rho_v^2 h_{fg}^2}{\rho_l^2 \sqrt{\alpha_l} C_{p,l} T_l} \tag{15}$$

Ehrlich and Murdock [25] further developed this parameter to a non-dimensional thermal scaling parameter called *Dimensionless Bubble* (DB) parameter by considering bubble

growth over a time-varying pressure field. The resulting DB parameter is similar to the formulation suggested by Ruggeri and Moore [20] and is considered very convenient for estimating the thermal operational boundaries of the test bench at an early stage in the test bench design process, as it is based solely on thermodynamic properties of the bulk fluid rather than empirical correlations. For the detailed investigation of a specific pump, it is of high importance to take into account all available prediction models, especially those for which better validation data is available in literature.

$$\mathrm{DB} = \frac{R_t \omega^{3/2} C_{p,l} T_l \rho_l^2 \sqrt{\alpha_l}}{h_{fg}^2 \rho_v^2} \tag{16}$$

3. TEST OBJECT

One main goal of the test bench under construction is to establish a result validation loop within the numerical design process for turbopumps at TUM. The pump to be developed is a liquid oxygen turbopump designed for a liquid hydrogen and liquid oxygen expander cycle engine. The desired operational parameters are given in Table 1. The resulting thrust level is in the order of magnitude of the VINCI upper stage engine.

Table 1. LOX turbopump nominal operating conditions

Property	Value	Unit
Rotational speed N	20000	rpm
Nominal mass flow rate $\dot{m}$	25	kg/s
Total pressure at pump inlet $p_{t,1}$	2.5	bar
Temperature at pump inlet T_1	90	K
Total pressure at pump outlet $p_{t,3}$	70	bar

A radial-type impeller was selected based on the suction specific speed N_{SS} value of the pump. Additionally, in order to avoid cavitation in the radial impeller stage, a high head inducer with cylindrical tip shape was positioned in front of the impeller. [1, 5] A summary of the design details at nominal operating conditions with liquid oxygen is given in Table 2.

A preliminary CAD sketch of the pump assembly with inducer, impeller and turbine is shown in Figure 2. The test bench is designed in such a way as to investigate the pump detached from the turbine system. The parts of the pump assembly that are relevant for the test bench design are highlighted.

4. TEST BENCH DESIGN

The main properties of the test bench can be selected based on the dimensions of the pump under development and the general scaling methods for pumps, which have both been introduced in the sections before. The following section identifies the test objectives which are of interest and the implementation in the test bench.

Table 2. LOX turbopump detailed design parameters

Property	Value	Unit
Pump Characteristics		
Specific speed N_S	24.34	$rpm \cdot m^2/\sqrt{s}$
Design head coefficient $\psi_{st,pump}$	0.56	-
Hydraulic efficiency η_{hyd}	0.88	-
Pump overall efficiency η_{tot}	0.75	-
Shaft power P_{shaft}	−197	kW
Inducer Characteristics		
Design suction specific speed N_{SS}	421.42	$rpm \cdot m^2/\sqrt{s}$
Design head coefficient $\psi_{tot,inducer}$	0.11	-
Design flow coefficient $\varphi_{inducer}$	0.089	-
Number of blades $Z_{inducer}$	2	-
Hub-to-tip ratio, inlet $D_{h,1}/D_{t,1}$	0.40	-
Hub-to-tip ratio, outlet $D_{h,2}/D_{t,2}$	0.64	-
Tip diameter $D_{t,1}$	70.83	mm
Impeller Characteristics		
Design head coefficient $\psi_{tot,impeller}$	0.50	-
Design flow coefficient $\varphi_{impeller}$	0.10	-
Number of blades $Z_{impeller}$	6	-
Tip-to-outlet ratio D_{t2}/D_{t3}	0.72	-
Hub-to-outlet ratio D_{h2}/D_{t3}	0.46	-
Tip diameter D_{t3}	100.284	mm

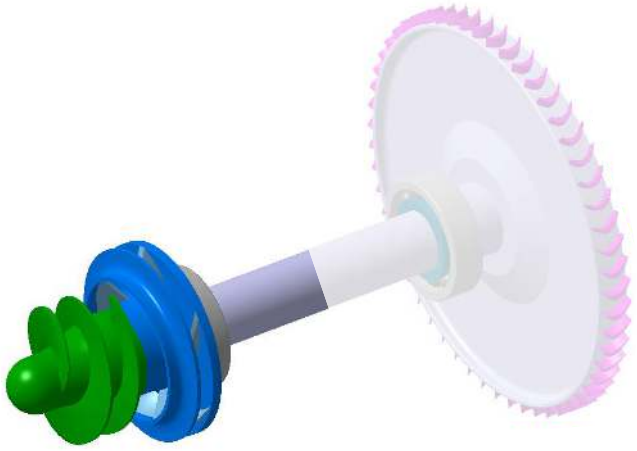

Figure 2. Preliminary CAD view of the developed turbopump at TUM without housing and volute. The pump components are highlighted.

4.1 Test Objectives

One of the key objectives of the test facility is to provide performance validation data for the turbopump development at the Division Space Propulsion, TUM. This can be yielded by measuring the pump's head rise at varied volume flow

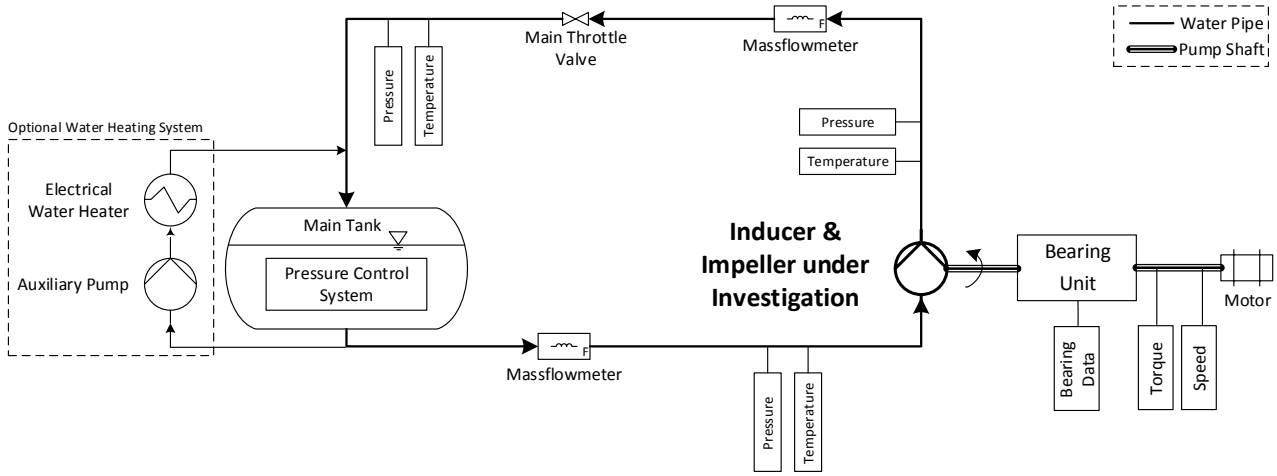

Figure 3. Drawing of the test bench layout

rates and rotational speeds in order to generate a pump performance chart. Therefore, it is necessary to acquire the following data: the pressure difference over the investigated pump, the mass flow rate, the shaft torque and the rotational speed of the shaft. The torque measurements give information about the efficiency of the pump under investigation. A second goal is to experimentally observe the cavitation behaviour of the inducer and the pump with water tests in order to predict the cavitation behaviour under liquid oxygen conditions. Therefore, as evident from the cavitation scaling theory, the water needs to be heated up in order to operate the facility with a liquid which is close to its boiling point.

4.2 Test Facility Dimensioning

For an operation of the pump in non-cavitating conditions, the scaling methods of equation 7, equation 8 and equation 9 have to be applied. The maximal rotational speed of the motor that drives the pump has been chosen to $N_{max} = 5500\,rpm$. The following considerations will approve this choice. Further, it is in good agreement with the rotational speeds of comparable test facilities. Consequently, sub-scale tests will be performed. The geometry stays the same as in the LOX hardware. The hardware designed for the LOX turbopump will be used on the test bench without any scaling: $\lambda_{geom} = 1$. The efficiency of the pump on the test bench and the efficiency of the original LOX pump are assumed to be equal: $\eta_m = \eta_a$.

With the properties of the pump under development at TUM, given in Table 1 and Table 2, the maximal mass flow rate at N_{max} based on the design point of the original LOX hardware calculates to

$$Q_{m,N_{max}} \approx \frac{Q_a N_{max}}{N_a} = 24.75\,{}^{m^3}/_{h} \tag{17}$$

The scaled design head rise at N_{max} equals

$$H_{m,N_{max}} \approx \frac{H_a {N_m}^2}{{N_a}^2} = 33.30\,m \tag{18}$$

At the same operating point, the shaft power calculates to

$$P_{m,N_{max}} \approx \frac{P_a {N_m}^3 \rho_m}{{N_a}^3 \rho_a} = 3.29\,kW \tag{19}$$

The dimensions of the new test facility have to be chosen in such a way that those parameters can be satisfied. A wider range of operation above those limits is desirable for potentially subsequent expansions of the test facility.
In order to test the cavitation performance of the pump inducer, it is necessary that the mass flow coefficient φ, the cavitation number σ and the thermodynamic properties match the ones of the LOX application. Further, the turbopump has to be operated in regions where $\mathrm{Re} > 10^6$. As for non-cavitating conditions, the geometry of the LOX hardware is used without dimensional scaling.
The minimal necessary rotational speed for which $\mathrm{Re} = 10^6$ is satisfied can be described, according to Equation 5, by

$$\omega \geq \frac{\upsilon \mathrm{Re}}{R_{t,3}^2} = 400.55\,{}^{rad}/_{s} \quad \text{or} \quad N \geq 3825.00\,rpm \tag{20}$$

The thermodynamic properties are assumed to be comparable if the Dimensionless Bubble (DB) parameter, as denoted in Equation 16, is equal or close to equal. For the LOX turbopump, with the operational parameters given in Table 1 and the dimensions of the impeller given in Table 2, this parameter calculates to $DB_{LOX,ref} = 0.306$ for the impeller of the TUM design. The plot in Figure 4 shows the LOX DB reference value $DB_{LOX,ref}$ as a constant line. Together with this constant value, the DB value calculated for different

rotational speeds is shown in dependence of the water temperature. It is clearly visible that for each rotational speed of the turbopump on the test bench, a specific water temperature has to be set in order to satisfy the equality of the *Dimensionless Bubble* (DB) parameter. With increasing rotational speed, the required water temperature rises. For the maximal chosen rotational speed of the motor N_{max}, the water temperature iteratively calculates to $T_{N_{max}} = 368\,K$. It has to be pointed out that this value for the bulk water temperature at the pump inlet only serves as design constraint to the water heating system at this early point in the test bench design procedure.

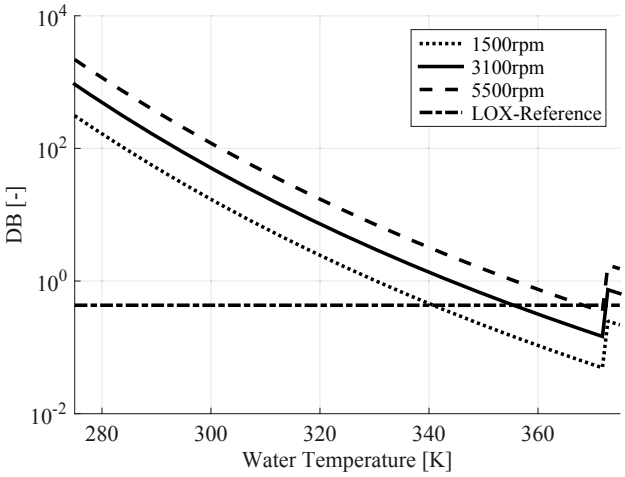

Figure 4. Dimenionless Bubble (DB) parameter at different rotational speeds. The DB reference value has been calculated for the a LOX pump as described in Table 1. The LOX geometry is used without any changes for the water tests. The DB values are calculated for $p_{t,1} = 1\,bar$.

4.3 Detailed Test Bench Design

Water is selected as the test medium. The use of water offers several advantages. The most important advantage is the easy handling. This allows for a comparably cheap operation of the test facility. Compared to tests with cryogenic fluids, the safety of tests is also improved. Further, only very few material incompatibilities are known. The system is designed as a closed circuit. This is especially advantageous for tests with heated water: after preheating the water up to the desired temperature, the heater only needs to keep the temperature at the desired level. This can improve the temperature control accuracy. The use of a closed water loop is also in good agreement with other test facilities for pumps at different institutes and national standards [6, 7, 8, 26, 27, 9, 10, 11, 28]. As the water is supposed to stay within the circuit for the duration of multiple test campaigns, deionized water is used. This is beneficial as depositions on water circuit components are limited. Especially for heated water, the sedimentary deposition of limescale is reduced significantly [29]. It has to be taken into account that the water needs a minimal conductivity greater $20\,\mu S/cm$ to guarantee the operation of inductive mass flow meters. The decay of the water quality is slowed down as well due to the fact that no permanent access of light is present in the system. A major drawback of a closed-loop system is that, in case of occurring cavitation, vapour bubbles can persist in the system and be sucked into the inlet again.

The drawing in Figure 3 shows an overview of the circuit. Necessary sensor positions, actuators and their positions within the loop are shown as well.

The water reservoir is realized by a stainless steel tank with a volume of $V_{tank} = 2000\,l$. It is designed to withstand the mechanical and thermal loads of water at $p_{tank,max} = 4\,bar$ and $T_{tank,max} = 100°C$. The tank is equipped with a EPDM membrane filled with pressurized air. This membrane has a volume of $V_{membrane} = 500\,l$. The air pressure within this membrane and therefore also within the tank is variable and can be controlled and regulated electronically. In operational modes where cavitation occurs, it is very likely that bubbles are transported into the tank and might disturb the pump measurements if they are sucked into the pump again. In order to significantly reduce this effect, it is desirable to maximize the residence time of the water in the reservoir. This is attained by redirecting the inlet flow in circumferential direction. In addition, the amount of dissolved oxygen can be measured in order to attain a good repeatability of the test conditions. Further, the tank can be depressurized up to a negative pressure of $p_{t,tank} = 0.9\,bar$ to remove dissolved oxygen. This is especially important for tests with heated water. For safety reasons, the tank is also equipped with an over-pressure valve. The controllable static inlet pressure allows to perform $NPSH_R$ evaluations on the test pump.

The inlet to the pump from the main reservoir and the outlet piping from the pump to the main tank is created by stainless steel tubes with circular cross-section and standard flange connectors. The tube dimension has been chosen to equal the standard dimension DN80. This results in an internal pipe diameter of all tubes of $D_{tube} = 80.8\,mm$. It is favourable to have a fully turbulent flow within the tubes present at all times. This is feasible with D_{tube} for mass flow rates from $\dot{m}_{min} = 0.6\,\frac{kg}{s}$ on. Based on the head rise scaling considerations in Equation 18, all tubes have been designed in the pressure class DN80-PN25. Due to restrictions of the sensors and auxiliary equipment in the loop, the static pressure in the inlet section, including the tank, is limited to $p_{1,max} = 4\,bar$. The pressure in the outlet section is limited to $p_{3,max} = 10\,bar$. In order to avoid possible sources of cavitation in the tubing, all transitions and redirections of flow are manufactured as smooth as possible. Further, all sources of flow disturbance are avoided in all tubes in front of sensors and in the tube in front of the pump inlet at a tube length of $L_{min} = 10\,D_{tube}$.

The head rise of the pump needs to be reduced to the pressure level of the tank. This is done by a throttle valve configuration in-between the pump and the tank. In order to reduce the risk of cavitation at the throttling system, two identical valves are arranged in a daisy-chain configuration. Both

valves are equipped with an electronically controllable actuation unit. This makes it possible to set the pressure drop across each valve independently. Further, the mass flow rate can be controlled. This feature is needed in order to do a performance mapping of the pump under investigation and it is a crucial requirement for cavitation scaling.

The mass flow rate is sensed at two locations. One inductive mass flow meter is placed in the inlet tubing directly in front of the pump inlet. A second inductive mass flow meter is placed after the pump. At the same position, a measurement orifice is placed. This is where the pressure drop across a defined through-flow area is measured. Thus, for a given fluid density, the mass flow rate can be calculated in a second, independent way. This allows for a comparison of measurement results and the improvement of the measurement accuracy in all measurement ranges.

For the controlled operation of the test bench, pressures and temperatures are captured at different locations of the water circuit. The static pressure is monitored, as depicted in Figure 3, in the pump inlet section, in the pump outlet section and directly after the main throttle valve configuration. At all three locations, the pressure measurements are averaged over the circumference of the horizontally placed pipes in order to compare for gravity effects. The measured static pressure difference between pump inlet and pump outlet can be used to calculate the head rise of the pump. The static pressure difference over the throttling valve configuration allows for a safe operation of the same. In addition, the tank pressure is also monitored. Additionally, temperatures are detected at all mentioned pressure sensor locations. Especially for tests with heated water, these temperature readings yield valuable information for the thermal control system.

The pump is driven by a three-phase alternating current (AC) electric motor with a maximal power of $P_{shaft,max} = 12\,kW$. The motor reaches its maximal torque $T_{shaft,max} = 27\,Nm$ at its design speed $N_{ref} = 3100\,rpm$. The maximal speed of the motor, without the use of any additional transmission, is $N_{max} = 5500\,rpm$. The motor is connected to the shaft by a flexible coupling that dampens the temporary high torque during start-up. The shaft is held in position by a bearing unit in overhung configuration - the bearings are positioned between the pump and the drive unit. The bearing unit is designed as an arrangement of a fixed bearing close to the pump and a floating bearing close to the drive unit. All loads on the drive unit are closely monitored. This includes the torque of the shaft, the rotational speed and the axial force acting on the fixed bearing. Further, a bearing monitoring system is established by permanent observation of the bearing race temperatures. All bearings are run with grease lubrication and the grease quality is observed in fixed intervals. Further, the pump housing is equipped with three acceleration sensors for the investigation of potential instabilities. The data obtained from those sensors can also be used to monitor the bearing operation.

As shown in section 2, in order to reproduce the cavitation behaviour of the LOX turbopump, it is necessary to run tests with heated water. Therefore, a water heating system is included in the test bench setup. This heating system is designed as a second auxiliary circuit that can be decoupled from the pump circuit. Thus, it is possible to heat the water contained in the main tank to a desired temperature. The water is heated up by an electrical heater with a power of $P_{ht,el} = 60\,kW$. The water in the second auxiliary water circuit is driven by a separate pump. The heating system is designed to control the temperature within $\Delta T_1 = \pm 1\,K$ and can attain a maximal water temperature of $T_{max} = 100°C$. For means of flow control in the auxiliary heating circuit, the water temperature at the heater outlet, the static pressure at heater inlet and heater outlet as well as the mass flow rate are closely monitored. The mass flow rate is detected by a measuring orifice. The bladder inside the main tank serves as a compensation reservoir for volumetric changes due to the heating of the water. A dedicated cooling system is not implemented, but the insulation of the tank and the tubing is designed in a way that continuous heating is necessary to attain a constant high temperature.
Figure 5 shows a CAD plot of the main circuit of the test facility that is currently being constructed at the Division Space Propulsion, TUM.

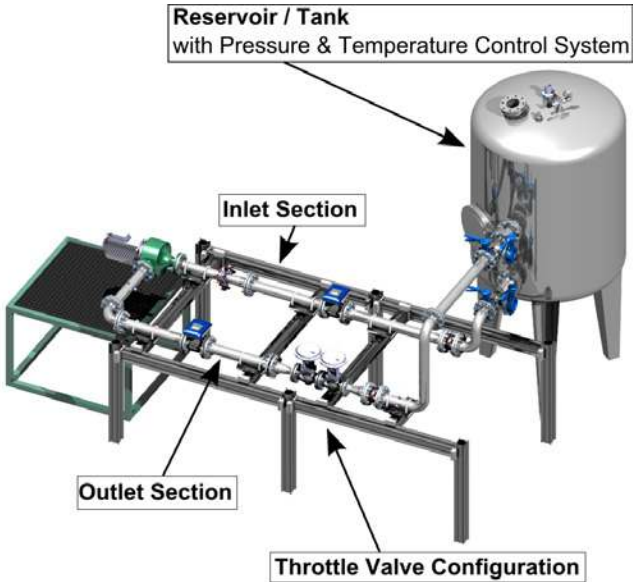

Figure 5. CAD view of the turbopump test bench at TUM

4.4 Numerical Design Methods

In order to enhance the test facility development described in the previous sections, the test bench was modelled numerically in parallel with the physical setup. Therefore, the water circuit including all pipes, valves and the tank have been modelled in the software tool *EcosimPro®*. Especially all components that are foreseen to be electronically controlled were investigated numerically in detail. Therefore, the heating system and the tank, including the membrane bladder, were represented as detailed numerical models. For all components, the pressure drop across those components

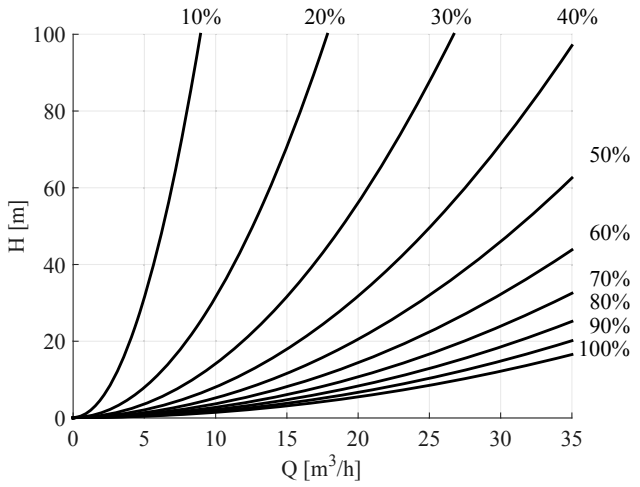

Figure 6. Numerically obtained system performance chart. The percentile values denote the level of opening of the throttle valve configuration.

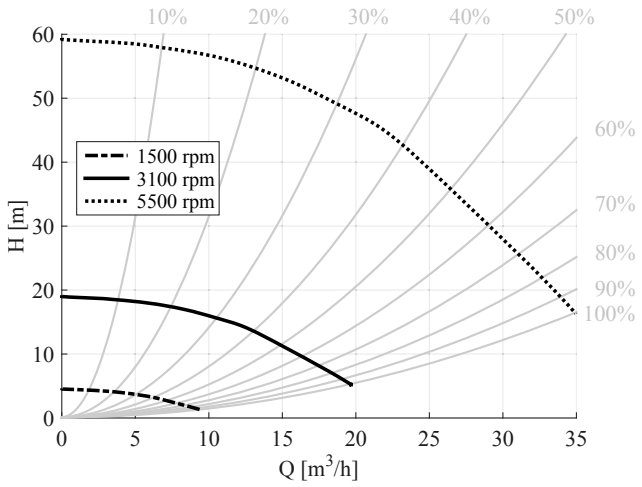

Figure 7. Numerically obtained pump performance chart for $N = 1500\,rpm$, $N = 3100\,rpm$ & $N = 5500\,rpm$. The system performance chart for different opening levels of the throttle valve configuration are plotted in gray.

is implemented for different mass flow rates as core functionality. Further, for investigations on the thermal control of the test bench, empirical correlations for heat losses at all surfaces have been added. The software suite *EcosimPro*® offers many tubing and piping elements readily available in its libraries that have been adapted to the properties of the test bench. They can be combined in a modular way. The *EcosimPro*® library *ESPSS* expands the building blocks by components for rocket engines. This includes special tank configurations as well as a generic turbopump model.

The graph in Figure 6 shows a numerically obtained system performance chart for different positions of the throttle valve assembly. For the generation of this chart, the throttle valve configuration was opened at a fixed percentage and the mass flow rate was varied. The static pressure at the pump inlet and the pump outlet was measured and the resulting head of the system was calculated. Especially the performance for the fully opened throttle valve configuration is of high interest as this curve describes the minimal head that a pump has to generate in order to be tested on the test bench.
Further, a numerical evaluation of the pump operation within the circuit has been evaluated. Therefore, the generic pump model has been initialized with a specific speed of $N_S = 24.34$, a total head of $H_{tot} = 602.3\,m$, the design rotational speed of $N_{LOX} = 20000\,rpm$ and an estimated efficiency of $\eta = 0.887$. The graph in Figure 7 shows the computed pump characteristic for $N = 1500\,rpm$, the motor design speed $N_{ref} = 3100\,rpm$ and the maximal rotational speed of the motor $N_{max} = 5500\,rpm$. Additionally, the system performance map is partially shown. This makes it possible to identify the resulting operation points. This chart has been created by varying the opening level of the throttle valve configuration from 0% to 100%. The rotational speed of the pump has been kept constant for each curve. The head rise across the pump has been measured.

5. SUMMARY AND OUTLOOK

The key characteristics of the developed test facility are summarized in Table 3. The designed test bench provides a valuable facility to test radial pumps with inducers in a sub-scale environment. According to the presented scaling methods, the results obtained here can be used to predict the non-scaled pump performance of the original application. Additionally, the possibilities to heat up the water, to control the flow rate and to control the inlet pressure separately, allow for the investigation of the occurrence of cavitation at the inducer blades.

Table 3. Operational Characteristics of the Test Facility at TUM

Property	Value	Unit
Rotational speed N	≤ 5500	rpm
Pump Power P	≤ 12	kW
Inducer Diameter $D_{t,1}$	≤ 80	mm
Impeller Diameter $D_{t,3}$	≤ 150	mm
Fluid Temperature T	≤ 100	°C
Total pressure at pump inlet $p_{tot,1}$	≥ 1	bar
Total pressure at pump outlet $p_{tot,3}$	≤ 10	bar
Cavitation Number σ	$0.02 \ldots 0.45$	-
Flow coefficient φ	≤ 0.11	-

The presented test facility has been designed to meet the test criteria for the LOX-turbopump which is currently under development here at TUM. All dimensions and characteristics of the components have been chosen accordingly. Nevertheless, the test bench can be used to investigate any pump of similar constructive form, as long as it stays within the constraints given in Table 3. Based on the Barber-Nichol's chart for pumps [30], the operational boundaries of the test

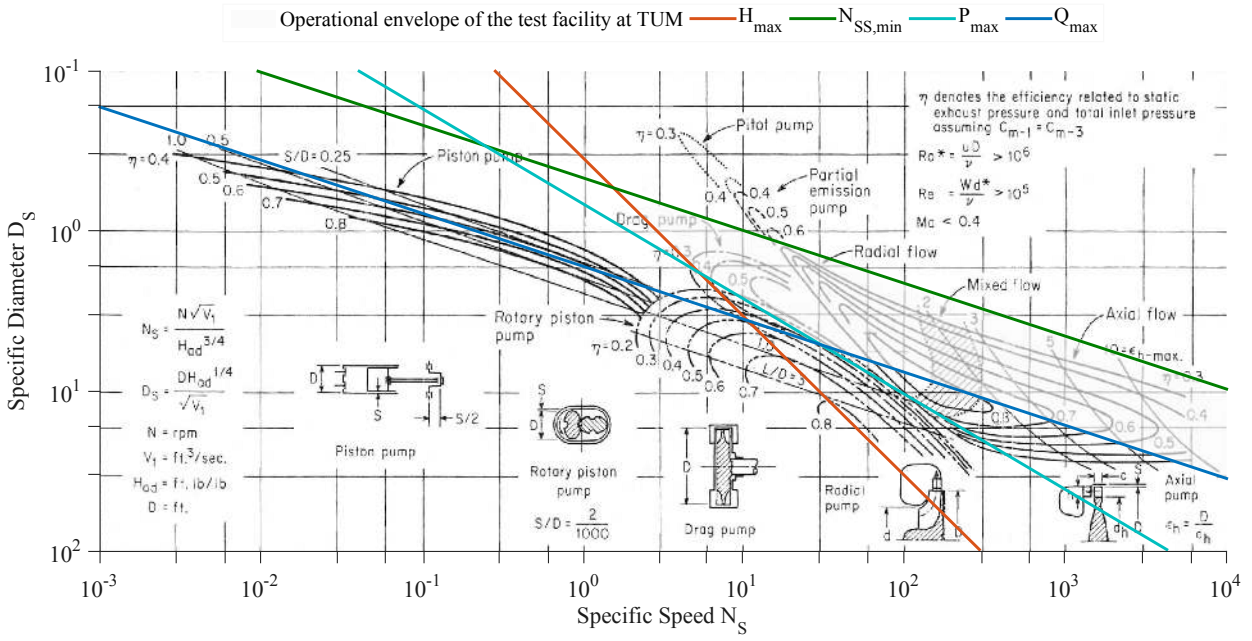

Figure 8. Operational envelope of the turbopump test facility at TUM [1]

[1] This figure is composed by overlaying the Barber Nichols chart for pumps [30] with the operational boundaries of the test facility at the Division Space Propulsion, TUM.

bench have been plotted in a Specific Speed - Specific Diameter ($N_S - D_S$) chart. The visualization of the boundaries is shown in Figure 8. For this figure, the maximal mass flow rate has been chosen to $\dot{m}_{max} = 25\,\frac{kg}{s}$. In general, the mass flow rate of the test facility is not limited, but, according to the system performance chart in Figure 6, the necessary minimal head rise of the investigated pump increases with increasing mass flow rate.

The numerical implementation of all components with *EcosimPro*® in parallel with the physical construction of the test facility has shown to be beneficial. It was possible to investigate component dimensions at question numerically and the a priori understanding of the test facility was greatly improved. Especially the dimensioning of the water heating system and the development of the inlet pressure control system in the tank were supported by numerical studies. Implementations of simple circuit components like straight and bent pipes, valves and tanks are available and the empirical correlations are of good quality for the full operating region of the test bench. The preliminarily calculated performance chart derived from the generic pump model shows the same order of magnitude as the analytically scaled values. Anyhow, especially the implementation of the pump, based on the generic pump component from the *ESPSS* library, does not yield the desired amount of details. Two possibilities have been identified in order to perform improved numerical analyses: (1) Experimental measurement of the pump performance map and implementing this information in a module or (2) detailed modeling of the single pump components. Both approaches are currently being followed at TUM. For the second approach, a detailed model of the inlet, the inducer, the impeller, the diffusor and the volute of the pump developed at TUM are under development.

NOMENCLATURE

Symbols

A	area
α	thermal diffusivity
C_p	specific heat
D	diameter
DB	Dimensionless Bubble parameter
η	efficiency
Eu	Euler number
F	force
Fr	Froude number
g	gravitational acceleration. $g = 9,81\,m/s^2$
H	head rise
h_{fg}	heat of vaporization
λ	scaling factor
$\dot{m}$	mass flow rate
N	rotational speed $\left[min^{-1}\right]$
N_S	specific speed. $N_S = N \cdot \frac{\sqrt{Q}}{H^{0.75}}$
N_{SS}	suction specific speed. $N_{SS} = N \cdot \frac{\sqrt{Q}}{NPSH^{0.75}}$
P	power
p	pressure
ψ	head coefficient. $\psi = {}^{2gH}/_{U_3^2}$
φ	flow coefficient
U	peripheral velocity
Q	volume flow rate

R	radius
ρ	density
Re	Reynolds number
Σ	cavitation parameter (Brennen)
T	temperature
υ	kinematic viscosity
v	velocity
ω	rotational speed [$^{rad}/_{s}$]
X	length
Z	number of blades

Subscripts

A	available
a	application prototype (not scaled)
c	characteristic
el	electrical
h	hub
ht	heating circuit
hyd	hydraulic
l	liquid
m	model for tests
R	required
SS	suction specific
st	static
t	tip
tot	total
v	vapor
1	inducer inlet
2	interface between inducer and impeller
3	impeller outlet

Abbreviations

NPSH	Net Positive Suction Head
AC	Alternating Current
CAD	Computer Aided Design
DB	Dimensionless Bubble parameter
LH_2	Liquid Hydrogen
LOX	Liquid Oxygen
LRE	Liquid Rocket Engine
TSH	Thermodynamic Suppression Head
TUM	Technical University of Munich

ACKNOWLEDGMENTS

This project is supported by the *Ludwig Bölkow Campus*, funded by the Bavarian government. The authors greatly appreciate the good cooperation with the consortium partners.

REFERENCES

[1] L. Veggi, J. D. Pauw, B. Wagner, T. Godwin, and O. J. Haidn. Numerical and experimental activities on liquid oxygen turbopumps. *Space Propulsion Conference*, 2016.

[2] B. Wagner, A. Stampfl, P. Beck, L. Veggi, J. D. Pauw, and W. Kitsche. Untersuchungen zu Sekundärsystemen in Turbopumpen für Flüssigkeitsraketenantriebe. *Space Propulsion Conference*, 2016.

[3] Ch. Wagner, T. Berninger, T. Thümmel, and D. Rixen. Rotordynamic effects in turbopumps for space propulsion systems - first minimal models and experimental validation. *Space Propulsion Conference*, 2016.

[4] Ch. Wagner, B. Proux, A. Krinner, T. Thümmel, and D. Rixen. Rotordynamik: Modellierung und Einfluss von Schrägkugellagern für Hochdrehzahlanwendungen. *Second IFToMM D-A-CH Conference*, 2016.

[5] L. Veggi, J. D. Pauw, B. Wagner, and O. J. Haidn. A study on the design of lox turbopump inducers. *Manuscript submitted for publication*, 2017.

[6] D. A. Ehrlich, J. Schwille, R. P. Welle, J. W. Murdock, and Hardy B. S. A water test facility for liquid rocket engine turbopump cavitation testing. *Proceedings of the 7th International Symposium on Cavitation*, 2009.

[7] E. Rapposelli, A. Cervone, Ch. Bramanti, and L. d'Agostino. A new cavitation test facility at centrospazio. *4th International Conference on Launcher Technology Space Launcher Liquid Propulsion*, 2002.

[8] E. Rapposelli, A. Cervone, and L. d'Agostino. A new cavitating pump rotordynamic test facility. *38th AIAA/ASME/SAE/ASEE Joint Propulsion Conference & Exhibit*, 2002. AIAA 2002-4285.

[9] J. Kim, H. H. Song, and S. J. Song. Measurements of the non-dimensional thermal parameter effects on cavitation in a turbopump inducer. *ISROMAC*, 2016.

[10] S.-L. Ng. Dynamic response of cavitating turbomachines. California Institute of Technology, 1976. Report No. E 183.1.

[11] Stephen Skelley. Summary of Recent Inducer Testing at MSFC and Future Plans. presentation, 2003. Thermal and Fluids Analysis Workshop, August 18-22, NASA/Marshall Space Flight Center.

[12] O. E. Balje. *Turbomachines: A Guide to Design, Selection, and Theory*. John Wiley & Sons, New York, 1981.

[13] H. Sigloch. *Strömungsmaschinen: Grundlagen und Anwendungen*. Hanser, München, 2013.

[14] J. F. Gülich. *Centrifugal Pumps*. Springer, Berlin Heidelberg, 2010.

[15] C. Pfleiderer and H. Petermann. *Strömungsmaschinen*. Springer, Berlin, 7 edition, 2005.

[16] R. A. van den Braembussche. Radial compressor design and optimization: March 2016. von Karman Institute, Rhode-Saint-Genèse, 1994.

[17] S. L. Ceccio and S. A. Mäkiharju. Experimental methods for the study of hydrodynamic cavitation. In L. d'Agostino and M. V. Salvetti, editors, *Cavitation Instabilities and Rotordynamic Effects in Turbopumps and Hydroturbines*, volume 575 of *CISM International Centre for Mechanical Sciences courses and lectures*, pages 35–64. Springer, Wien, New York, 2017.

[18] Liquid rocket engine turbopump inducers. NASA Space Vehicle Design Criteria (Chemical Propulsion), 1971. NASA SP-8052.

[19] H. A. Stahl and A. J. Stepanoff. Thermodynamic aspects of cavitation in centrifugal pumps. *Journal of Basic Engineering*, 78:1691–1693, 1956.

[20] S. R. Ruggeri and R. S. Moore. Method for prediction of pump cavitation performance for various liquids, liquid temperatures, and rotation speeds. NASA Technical Note, 1969. NASA TN D-5292.

[21] H. Kato, H. Yamaguchi, K. Okada, S.and Kikuchi, and M. Myanaga. Suppression of sheet cavitation inception by water discharge through slit. *International Symposium on Cavitation Inception*, 1984.

[22] S. Watanabe, T. Hidaka, H. Horiguchi, A. Furukawa, and Y. Tsujimoto. Analysis of thermodynamic effects on cavitation instabilities. *ASME Journal of Fluids Engineering*, 129(9):1123–1130, 2007.

[23] J. P. Franc and C. Pellone. Analysis of thermal effects in a cavitating inducer using rayleigh equation. *ASME Journal of Fluids Engineering*, 129(8):974–983, 2007.

[24] C. E. Brennen. *Hydrodynamics of Pumps*. Oxford science publications. Concepts ETI, Norwich, Vt., 1994.

[25] D. A. Ehrlich and J. W. Murdock. A dimensionless scaling parameter for thermal effects on cavitation in turbopump inducers. *Journal of Fluids Engineering*, 137(4), 2015.

[26] C. Bramanti. *Experimental study of cavitation and flow instabilities in space rocket turbopumps and hydrofoils*. doctoral thesis, Università degli Studi di Pisa, 2006.

[27] A. Pasini. *Pumping Performance Similarity, Cavitation-Induced Instabilities and Fluid-Induced Rotordynamic Forces in Tapered Inducers*. doctoral thesis, Università degli Studi di Pisa, 2010.

[28] DIN EN ISO 9906. Rotodynamic pumps – Hydraulic performance acceptance tests – Grades 1, 2 and 3. German version EN ISO 9906:2012, 2013. DIN Deutsches Institut für Normung e.V. Beuth Verlag, Berlin.

[29] H. Bendlin. *Reinstwasser von A bis Z : Grundlagen und Lexikon*. VCH, Weinheim [u.a.], 1995.

[30] E. Kenneth and P.E. Nichols. How to select turbomachinery for your application. Barber-Nichols Inc.